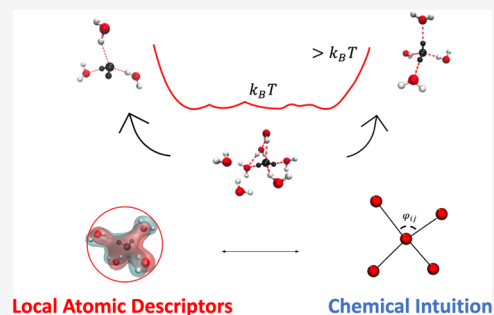


# High-Dimensional Fluctuations in Liquid Water: Combining Chemical Intuition with Unsupervised Learning

Adu Offei-Danso, Ali Hassanali,\* and Alex Rodriguez\*

**ABSTRACT:** The microscopic description of the local structure of water remains an open challenge. Here, we adopt an agnostic approach to understanding water's hydrogen bond network using data harvested from molecular dynamics simulations of an empirical water model. A battery of state-of-the-art unsupervised data-science techniques are used to characterize the free-energy landscape of water starting from encoding the water environment using local atomic descriptors, through dimensionality reduction and finally the use of advanced clustering techniques. Analysis of the free energy under ambient conditions was found to be consistent with a rough single basin and independent of the choice of the water model. We find that the fluctuations of the water network occur in a high-dimensional space, which we characterize using a combination of both atomic descriptors and chemical-intuition-based coordinates. We demonstrate that a combination of both types of variables is needed in order to adequately capture the complexity of the fluctuations in the hydrogen bond network at different length scales both at room temperature and also close to the critical point of water. Our results provide a general framework for examining fluctuations in water under different conditions.



## INTRODUCTION

Water is one of the most ubiquitous solvents found in numerous physical, chemical, biological, and even technological contexts.<sup>1–3</sup> Unlike most simple liquids, it is characterized by various thermodynamic and dynamical anomalies, such as an enhancement in its compressibility upon supercooling.<sup>4–6</sup> Its unique properties are rooted in its ability to form a directed hydrogen bond network.<sup>7,8</sup> Despite long study, the origins of these anomalies in terms of the underlying structure and dynamics of hydrogen bonds continue to be a topic of lively discussion.<sup>4,9–11</sup>

Perhaps one of the most debated issues in aqueous sciences over the last two decades has been how its instantaneous local structure evolves as a function of temperature and pressure.<sup>12</sup> Over a century ago, Roentgen proposed that the anomalies of water could be rationalized as a competition between two different water structures, namely, a low-density liquid (LDL) and a high-density liquid (HDL).<sup>13</sup> Since then, various experiments<sup>14–16</sup> and numerical simulations<sup>8,17–19</sup> have attempted to provide a microscopic picture of the structure of water, leading to contradictory conclusions. Very recently, there have been several reports proving the existence of a second critical point in water under supercooling with classical atomistic models.<sup>20,21</sup> These simulations on the timescales of tens of microseconds show transitions between LDL and HDL.

Several molecular simulations have tried to illustrate the possibility of the existence of the two state picture also in room-temperature water by examining the inherent structure of the liquid at zero-K.<sup>18,22,23</sup> The idea of liquid water

consisting of two co-existing liquids is invoked to rationalize various spectroscopic measurements of water.<sup>16,24</sup> On the other hand, most molecular dynamics simulations of water at room temperature show that it is a homogeneous liquid<sup>9,25</sup> and that any heterogeneities in its structure arise from transient short-lived fluctuations.<sup>25–27</sup> At the heart of understanding this problem lies the question of the discovery of molecular probes of the local environments in a disordered liquid medium, and subsequently, how to capture highly complex patterns in the hydrogen bond network on different length scales.

Over the last three decades, since the advancement in the use of computer simulations, a wide plethora of different reaction coordinates or order parameters have been constructed to interrogate local environments in water. These include, to name a few, the tetrahedrality ( $q_{tet}$ ),<sup>28,29</sup> local-structure index (LSI),<sup>30</sup> the distance of the fifth closest water molecule ( $d_5$ ) to a central water,<sup>31–33</sup> and local coordination defects.<sup>34–37</sup> Besides variables that quantify correlations in the water network, there have also been measures to quantify local density using variations of the Voronoi volumes, which probes the free space in the network and hence the density.<sup>10,25,38–41</sup>

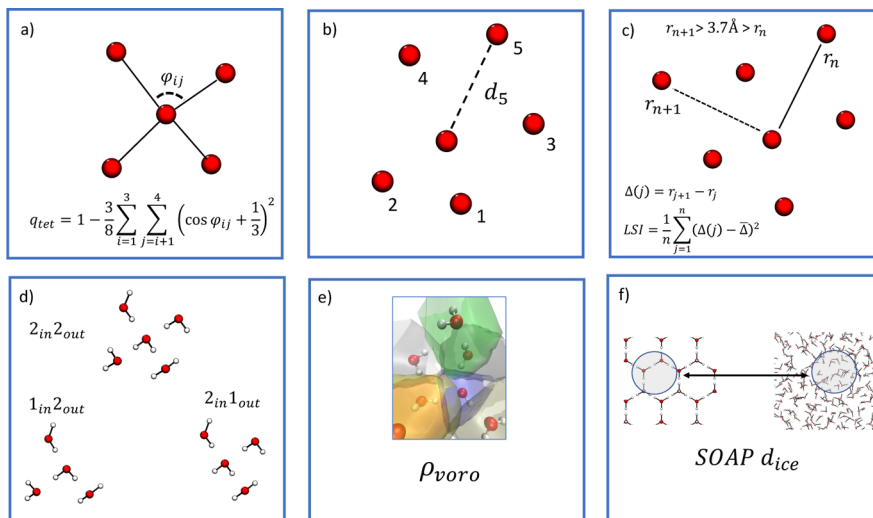


**Figure 1.** Visual schematic summarizing all the one-dimensional descriptors of water environments that were used in this work. (a)  $q_{tet}$  tetrahedrality associated with the four nearest neighbors. (b)  $d_5$ , distance from the fifth nearest neighbor. (c) LSI, local structure index measuring the extent of order/disorder between first and second solvation shells. (d) Topological defects in water. There are some examples shown, including  $2_{in}2_{out}$ ,  $1_{in}2_{out}$ , and  $2_{in}1_{out}$  water molecules. The in and out subscript correspond to the number of hydrogen bonds, being accepted/donated, respectively, by the central water molecule (e)  $\rho_{voro}$ , local density estimated as the inverse of the Voronoi volumes corresponding to each water molecule. (f) SOAP  $d_{ice}$  is the distance in the SOAP space from a given liquid water environment to the one present in hexagonal ice.

All these various quantities are inspired by chemical intuition and are used to infer differences between ordered and disordered water environments. The vast majority of these quantities are designed using cutoffs in the number of water molecules, such as in  $q_{tet}$  or  $d_5$  or radially defined thresholds in the case of the LSI. If water is seen as a percolating directed liquid network with medium-to-long range correlations beyond the first solvation shell, the ability of these chemically inspired parameters to capture all the complexities of the water network remains an open question.

In this work, we employ a series of state-of-the-art data-science techniques to investigate the fluctuations underlying the free-energy landscape of the TIP4P/2005<sup>42</sup> model of liquid water at room temperature and also close to the critical point. Our strategy is implemented in three steps and lays the groundwork for a general framework through which fluctuations of water in different contexts may be studied. First, we encode the information of water environments using a recently developed atomic descriptor, the smooth overlap of atomic positions (SOAPs) which has the power of preserving rotational, permutational, and translational invariances.<sup>43</sup> This is used to compare water environments on different length scales and topologies to important milestones such as ice.<sup>44</sup>

In the second step, the dimension of the manifold, in which the SOAP descriptors lie, is estimated using the two nearest neighbors intrinsic dimension estimator (TWO-NN).<sup>45</sup> This quantity, known as the intrinsic dimension (ID), has been successfully used to characterize the changes in the conformation of proteins<sup>46,47</sup> and phase transitions in simple classical and quantum Hamiltonians.<sup>48,49</sup> The ID also feeds into the third and final step of our procedure, in which the minima and transition states of the high-dimensional free-energy landscape are located using a density peak clustering algorithm.<sup>50–52</sup>

This procedure illustrates that at room temperature, the free-energy landscape associated with the local environment of water consists of one broad minimum that expands in several

dimensions. This feature is reproduced using both TIP4P/2005 and the many-body MB-pol potential.<sup>53</sup> The fluctuations of the hydrogen bond network within this single minimum free-energy landscape, however, occur in a high-dimensional space involving the coupling of many different degrees of solvent coordinates. We find that most of the chemically inspired variables such as  $q_{tet}$ , LSI, and  $d_5$  do not adequately describe the environments of water in terms of their apparent LDL or HDL character. Instead, combining these variables with the SOAP-based descriptors provides a much more nuanced picture underlying the fluctuations. Specifically, we show that the relevant variables needed to describe the fluctuations of water require both the oxygen and hydrogen atoms and that there are important hydrogen bonding interactions between the first and second solvation shell that affect the ID. These features are not always captured by coordinates such as  $d_5$  and LSI. We also explore how the SOAP descriptors evolve close to the critical point based on analysis of long trajectories in a recent work by Sciortino and Debenedetti.<sup>20</sup> This also provides new insights into the complexity of the hydrogen-bond fluctuations in the super-cooled regime.

The paper is organized as follows. We begin in [Section 1](#) with a description of all the computational methods used. In [Section 2](#), we report all on all our results where we discuss our findings of the intrinsic dimensionality of the hydrogen bond network, the free-energy landscape of liquid water at room temperature, and the molecular origins of the associated high-dimensional fluctuations. Within the results, we also elucidate the behavior of the high-dimensional fluctuations close to the critical point. Finally, we end with some conclusions and perspectives.

## METHODS

**Molecular Dynamics Simulations.** All-atom molecular dynamics simulations (MD) of 1019 water molecules were performed using the GROMACS 5.0 package.<sup>54</sup> For most of the results we report in this paper, we use the TIP4P/2005<sup>42</sup>

rigid water model. Besides this water model, we also compare some of our results with the MB-pol potential, which is one of the most accurate in silico potential reproducing many of the thermodynamic, dynamical, and spectroscopic properties of water across the phase diagram.<sup>53,55</sup> Energy minimization was first carried out to relax the system, followed by an *NVT* and *NPT* equilibration at 300 K and 1 atm for 10 ns each. A timestep of 2 fs was used for all the simulations. The *NVT* simulations were performed using the velocity-rescaling thermostat<sup>56</sup> with a time constant of 2 ps, while the *NPT* runs were conducted using the Parrinello–Rahman<sup>57</sup> barostat using a pressure coupling time constant of 2 ps. The production run at 300 K was carried out for 50 ns<sup>58</sup> in the *NPT* ensemble.

Besides the simulations at 300 K, we also analyzed molecular dynamics trajectories of supercooled water reported recently by Debenedetti and Sciortino, which showed for the first time, that atomistic models such as TIP4P/2005 and TIP4P/ICE<sup>59</sup> also display a second critical point. In these simulations, one observes fluctuations between high and low density phases of water. For more details on how these trajectories were generated, the reader is referred to the original manuscript.<sup>20</sup>

**Descriptors for Water Environments.** As eluded to earlier, we use a combination of both chemical-intuition and data-science-based descriptors to probe the local environment of water. While the former have been used to study the structure of water under different thermodynamic conditions,<sup>9,32,60</sup> the latter have been mainly developed for use in machine-learning applications.<sup>61,62</sup> In the following, we will detail the essential principles behind the descriptors used in this work (as summarized in Figure 1).

**Chemical-Based Descriptors.** Tetrahedrality ( $q_{\text{tet}}$ , Figure 1a) measures the similarity between the first-layer environment and a tetrahedron. It takes as an input the angles computed, taking as vertex the oxygen atom of the central water and all the possible couples generated by the four nearest neighbors, yielding a value of 1 for a perfectly tetrahedral environment.<sup>63,64</sup> The  $d_5$  parameter (Figure 1b) is the distance from the fifth nearest neighbor to the central atom and reflects the extent of separation between the first and second solvation shells. A larger value of  $d_5$  is interpreted as being a more open and locally ordered structure.<sup>33</sup> Figure 1c shows the functional form used to measure the LSI, which is designed to probe the order in the first and second coordination shells. By examining all but water molecules within a cutoff of 3.7 Å and the first molecule greater than this distance, the LSI distinguishes environments with a well-separated first and second coordination shells, from those that are more disordered.

All these variables do not explicitly include the hydrogen atoms. Numerous previous theoretical studies have shown that there are important correlations in the hydrogen bond network created by the local topology, which involves directed hydrogen bonds between water molecules.<sup>34,37,41,65</sup> Figure 1d shows some examples of topological defects that can be created from the canonical  $2_{\text{in}}2_{\text{out}}$  (two hydrogen bond donor and two acceptor) water, which we also examine in our work.

Although the previously described parameters are often interpreted in terms of high- and low-density environments, this can only be inferred indirectly. To obtain a more quantitative measure of density variations, we computed the Voronoi density ( $\rho_{\text{voro}}$ ), as illustrated in Figure 1e.  $\rho_{\text{voro}}$  is computed as the inverse of the Voronoi volume associated

with a water molecule, which is the sum of the volume of the oxygen and two hydrogen atoms.<sup>10,25,38</sup>

**Smooth Overlap of Atomic Positions.** Finally, Figure 1f shows the last one-dimensional descriptor that we used in this work, namely, the SOAP distance from a hexagonal ice structure. This variable quantifies how different a local water environment in liquid water is from a water molecule obeying the ice rules in the ice lattice. Depending on the choice of the various SOAP parameters, one can generate a wide variety of distance measures. Since the application of these types of descriptors in the study of condensed phase systems is quite new, we provide a more detailed discussion of the method next.

As indicated earlier, local atomic descriptors such as SOAPs preserve important symmetries such as rotational, permutational, and translational invariances when comparing different environments. The SOAP descriptor, in particular, has successfully been applied in various contexts such as characterizing hydrogen bond networks<sup>30</sup> in biological systems,<sup>66–68</sup> inorganic crystals,<sup>69,70</sup> and also very recently in liquid water.<sup>44</sup>

Given a particular atomic species  $Z_i$ , one characterizes its local environment as a sum of Gaussian functions with variance  $\sigma^2$  centered on each of the neighbors of a central atom including the central atom itself

$$\rho^{Z_i}(\mathbf{r}) = \sum_j \exp\left(\frac{-|\mathbf{r} - \mathbf{r}_{ij}|^2}{2\sigma^2}\right) \quad (1)$$

This atomic neighbor density can be expanded in a basis of radial basis functions and spherical harmonics, as illustrated below

$$\rho^{Z_i}(\mathbf{r}) \approx \sum_{n=0}^{n_{\text{max}}} \sum_{l=0}^{l_{\text{max}}} \sum_{m=-l}^l c_{nlm}^{Z_i} g_n(r) Y_{lm}(\theta, \phi) \quad (2)$$

where  $c_{nlm}^{Z_i}$  denotes the coefficients. Given  $\rho^{Z_i}(\mathbf{r})$ , one can obtain the coefficients as

$$c_{nlm}^{Z_i} = \int \int \int_{\mathcal{V}} dV g_n(r) Y_{lm}(\theta, \phi) \rho^{Z_i}(\mathbf{r}) \quad (3)$$

The number of coefficients of the basis functions, one chooses to compute, is bounded by the number of radial basis functions  $n_{\text{max}}$  and that of the angular basis functions  $l_{\text{max}}$ . The parameter  $r_{\text{cut}}$  identifies all atoms within some radial cutoff of the central atom. One can then define a rotationally invariant power spectrum as

$$p_{nn'l}^{Z_1 Z_2} = \pi \sqrt{\frac{8}{2l+1}} \sum_m c_{nlm}^{Z_1} \times c_{n'l m}^{Z_2} \quad (4)$$

By accumulating the elements of the power spectrum into a vector  $\mathbf{p}$ , the distance between two environments  $\chi$  and  $\chi'$  is related to the SOAP kernel by the following expression

$$d(\chi, \chi') = 1 - K^{\text{SOAP}}(\mathbf{p}, \mathbf{p}') \quad (5)$$

where

$$K^{\text{SOAP}}(\mathbf{p}, \mathbf{p}') = \left( \frac{\mathbf{p} \cdot \mathbf{p}'}{\sqrt{\mathbf{p} \cdot \mathbf{p} \mathbf{p}' \cdot \mathbf{p}'}} \right) \quad (6)$$

For our simulations of bulk water, the SOAP descriptor for a water molecule is constructed involving different combinations

of the oxygen and hydrogen atoms and their environments. The first descriptor, ( $\vec{O}$ ), is formed by computing the power spectrum of the density constructed by placing Gaussian functions on only the oxygen atoms within a certain radius centered about the position of the oxygen of the central water molecule. The other two descriptors include the hydrogen atoms of the water molecule. Since a water molecule contains two hydrogen atoms, it is necessary to choose the centers in a way that would make new descriptor invariant to the permutation the two indices. This was achieved by averaging the power spectra generated with centers on each of the hydrogen atoms ( $\vec{H}_{\text{ave}}$ ). In order to preserve information about the possible asymmetries present in the environment of the two hydrogen atoms, the absolute value of the difference in the descriptors was also considered ( $\vec{H}_{\text{dif}}$ ). Using these soap descriptors, we focused the ensuing analysis on three variations:  $\vec{O}$ , ( $\vec{O}$ ,  $\vec{H}_{\text{ave}}$ ), and finally ( $\vec{O}$ ,  $\vec{H}_{\text{ave}}$ ,  $\vec{H}_{\text{dif}}$ ).

The SOAP descriptors were constructed using the Dscribe package.<sup>71</sup> In practice, 10 randomly chosen water molecules were selected from each frame with a sampling frequency of 4 ps. This was carried out to ensure the independence of points by reducing the effects of spatial and temporal correlations between sampled environments. In total, 120,000 points were extracted for a radial cutoff of 3.7 and 6.0 Å. These cutoffs were chosen to enclose the first and second hydration shell of water, respectively. Our analysis was carried out using 8 ( $n_{\text{max}}$ ) radial and 6 ( $l_{\text{max}}$ ) angular basis functions. These values are similar to those used in previous studies.<sup>44,69</sup> With the power spectrum of the SOAP-based environments in hand, one can compute distances between the different local environments in water and other milestone structures, for example, ice. In this work, for most of our analysis, we focus on comparing the local environments in water to those in hexagonal ice although. In the rest of the manuscript, this distance is referred to as  $d_{\text{ice}}$ . One can also select many different milestone structures to compare with. For example, Petersson and co-workers have recently proposed the possibility of low-density liquid environments arising from fused dodecahedron structures.<sup>72</sup> SOAP distances can then be constructed with respect to this structure. When this is done, we will make reference to this distance as  $d_{\text{dod}}$ . Cheng et al. and Pavan et al. recently used SOAP-based descriptors to compare environments in water to different phases of ice by building an average SOAP kernel,<sup>44,73</sup> which allows for examining changes in the global structure. However, it should be stressed that while building average descriptors is sufficient for describing the global properties of phases, averaging over all the environments washes out important details on the local molecular structure.

**Data-Science Protocol.** Extracting the SOAP descriptors, as outlined previously, results in high-dimensional power spectra. Specifically, the dimensions for the three SOAP descriptors outlined earlier, are 252, 504, and 2856 for  $\vec{O}$ , ( $\vec{O}$ ,  $\vec{H}_{\text{ave}}$ ), and ( $\vec{O}$ ,  $\vec{H}_{\text{ave}}$ ,  $\vec{H}_{\text{dif}}$ ), respectively. The high dimensionality of these spectra implies the need of using advanced techniques to extract the meaningful information. In the following, we review the data-mining techniques that we employed.

**Intrinsic Dimensionality (ID).** In high-dimensional data, the existence of correlations between the different variables describing each data point implies that the system of interest likely resides in a lower dimensionality landscape. Take for example, a set of points in three dimensions—if they are distributed randomly, the ID would be three. However, correlations between the coordinates could result in the data

points lying only on the surface of the sphere, which would in turn lead to an ID of 2. Computing the ID is closely related with dimensionality reduction techniques,<sup>74–76</sup> in which the data set is projected into a lower dimensional space for data analysis, visualization, and interpretation. The ID represents the minimum dimensionality, in which these techniques can be employed without an important information loss. A correct knowledge of the ID should inform the choice of the space one examines the fluctuations of the system. In the case of our study, the ID plays an important role in estimating a point-dependent density function, which ultimately affects the extraction of the free energy as outlined later.

In this work, we made use of a recently developed technique namely the Two-NN estimator,<sup>45</sup> which estimates the ID based on information of the first and second nearest neighbor of data points. The method has been successfully applied in studying different molecular systems.<sup>40,46,77</sup> The main ideas are sketched below. Assuming local uniformity of the data set, it can be shown that the ratio of the second nearest neighbor and the first nearest neighbor distances ( $\mu = r_2/r_1$ ) yields the following distribution

$$P(\mu) = \frac{d}{\mu^{d+1}} \quad (7)$$

where  $d$  is the ID. Assuming all sampled ratios that  $\mu_i$ s are independent, it can be shown that the ID can be estimated using the following formula

$$d = \frac{N}{\sum_i \log(\mu_i)} \quad (8)$$

Using the SOAP distances, we estimated the ID of the environment around a water molecule. The physical significance of the ID is that it corresponds to the minimum number of independent order parameters or reaction coordinates required to describe, in our case, the environment around a water molecule. In this way, one can also quantify using the ID, the amount of information that is gained or lost when including different variables.<sup>78</sup>

**High-Dimensional Free Energy and Clustering.** Constructing the free-energy landscape of water requires an understanding of the relevant variables that characterize its underlying structural fluctuations. One of the common strategies in this context is to look at the probability densities along variables such as those introduced earlier like  $q_{\text{tet}}$ , LSI and  $d_3$ .<sup>23,30,31</sup> However, this implicitly assumes that there is no information loss when this projection is carried out, and furthermore, that the variable correctly encodes for the physical or chemical processes that one is interested in. In the last two decades, there has been a growing number of advanced techniques developed to automatically identify important degrees of freedom<sup>79,80</sup> and construct free energies in high dimensions.<sup>51,81–84</sup> For a more elaborate discussion of these techniques, the interested reader is referred to a recent review on the topic.<sup>85</sup>

In this work, we employ a recently developed Point Adaptive K-nearest estimator (PAK)<sup>51</sup> that avoids the need of any projection and has been used to study a wide variety of complex molecular systems.<sup>46,47,77</sup> In brief, the method uses the ID as a parameter to construct a point-dependent density ( $\rho_i$ ). This density is computed by adding a linear correction to the standard  $k$ -nearest neighbor estimator, in which the density is computed as  $\rho_i = \frac{k_i}{r_i^{k_i}}$  and the  $k_i$ s are chosen in order to



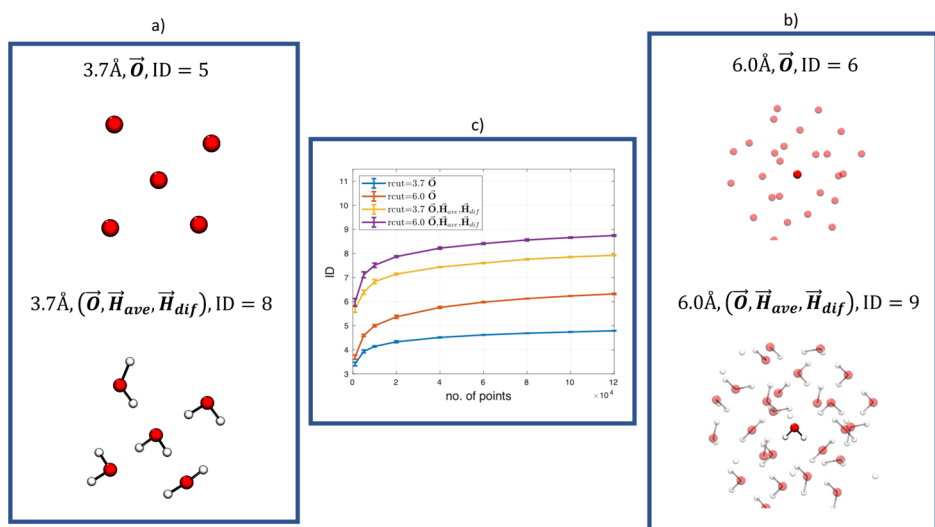


**Figure 2.** (a) 3.7 Å environment involving only oxygen atoms (top) and the same environment with hydrogen atoms (bottom). The intrinsic dimensionality is found to increase by 3 when hydrogens are included. (b) 6.0 Å environment involving only oxygen atoms (top) and the same environment with hydrogen atoms (bottom). The intrinsic dimensionality is found to increase by 3 when hydrogens are included. (c) Scaling of the intrinsic dimensionality with the number of points of the data set.

minimize the errors in density. The point-dependent free energy is then taken to be  $-\text{Log}(\rho_i)$ . Previous work has shown that this methodology works very well at providing accurate estimates of the errors in free energy up to dimensions as large as 8.<sup>51</sup>

With the point-dependent free energies in hand, the independent minima in the free-energy landscape (the clusters) are determined using a form of the modified density peak clustering algorithm (DPA).<sup>52</sup> This is an unsupervised extension of the original density peak clustering,<sup>50</sup> which automatically determines the clusters keeping only those that are statistically significant using a confidence interval  $z$ . Unless otherwise stated, the  $z$ -value chosen for most of the analysis presented is set to 2.5.

Finally, the results of PAK and DPA have been visualized and interpreted with the help of the uniform manifold approximation and projection (UMAP).<sup>86</sup> UMAP provides a convenient way of visualizing the high-dimensional free energy in two dimensions and has been carried out in several recent applications.<sup>87</sup>

## RESULTS AND DISCUSSION

**ID Analysis of the Hydrogen Bond Network.** Using the Two-NN estimator, we extracted the ID of the hydrogen bond network using the SOAP descriptors described earlier. In the context of water fluctuations, the ID provides a quantitative measure of the changes in the information content on adding several features when describing the local water environment. Specifically, in our analysis, we systematically examine how the ID changes when increasing the cutoff from layer 3.7 Å to the second 6.0 Å and when adding hydrogen atoms to the descriptors.

Figure 2 summarizes the results obtained from ID analysis. Panel (a,b) schematically illustrates the local environments that are included with the corresponding inferred IDs. Panel (c) shows the convergence of the ID as a function of the number of data points. Essentially, the ID can be increased in two possible ways: first by including or excluding the chemical species in a water molecule, namely, oxygen or hydrogen

atoms, and second, by increasing the size of the solvation shell of the local water environment.

Interestingly, ID analysis shows there is a much bigger change in the importance of including hydrogen atoms into the descriptors compared to expanding the radial cutoff. For both the 3.7 and 6 Å radial cutoffs, the ID increases by 3 upon the inclusion of the hydrogen atoms. On the other hand, moving from the smaller to larger radial cutoff increases the ID by a unit value. Several of the chemical-based order parameters described earlier in Figure 2, for example,  $q_{\text{tet}}$ ,  $d_s$ , and the LSI do not explicitly include the hydrogen atoms and therefore are very likely to miss out important coordinates needed to characterize the water environments.

To understand better the molecular origins of these differences in the ID, one can examine the effect of the inclusion of the hydrogen atoms when comparing different water environments. For instance, we can take the two defects that are shown in Figure 1 panel (d), namely,  $1_{\text{in}}2_{\text{out}}$  and  $2_{\text{in}}1_{\text{out}}$  and compute the distribution of the SOAP distances within each class of defect type and between the two defects. In Figure S1, it can be seen that when using only the oxygen atoms ( $\vec{O}$ ), the distributions within and across different defects are almost identical. However, upon adding the hydrogen atom contributions ( $\vec{O}, \vec{H}_{\text{ave}}, \vec{H}_{\text{dif}}$ ), the distributions are different with a slight bias toward higher values in the case of the intergroup distance distributions. Although there is clearly significant overlap in all these distributions, our analysis shows that by only using ( $\vec{O}$ ), there is important information about the hydrogen bond network that is lost.

The changes in the ID have important implications on our understanding of the free-energy landscape of water. First, the hydrogen bonds between water molecules involve directed dipole-dipole interactions which arise from the asymmetry in the position of the hydrogen atoms. This feature of the chemistry is clearly reflected in the change in the ID upon including the hydrogen atoms. At the same time, the presence of medium-to-longer range structural and orientational correlations in the network are manifested also in the increase in the ID albeit to a smaller extent than the role of directionality.<sup>88</sup> In some sense, the enhancement in the ID

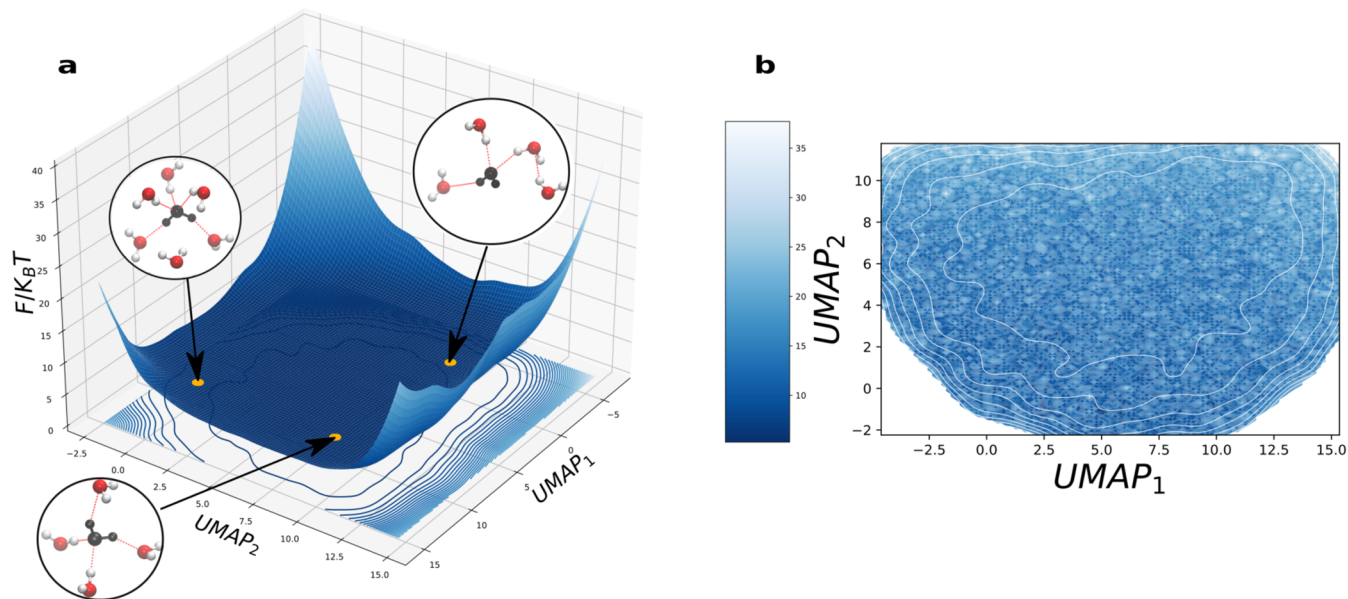


**Figure 3.** (a) FES constructed in 2D UMAP manifold reveals a single basin. Also shown are three different water environments which are separated by no significant barriers, indicating that fluctuations between different structures occur within a flat free-energy landscape. (b) Contour plot of the 2D UMAP manifold colored by the actual free-energy values is also consistent with a rough but rather flat basin.

from the oriented hydrogen bonds within 3.7 Å is strongly coupled to the order or disorder at longer distances.

In addition to the effect of the ID on the combination of the variables, as shown in Figure 2, we also examined the effect of the two hydrogen atom-based SOAP descriptors, namely,  $\bar{H}_{\text{ave}}$  and  $\bar{H}_{\text{dif}}$ . For both the 3.7 and 6.0 Å environments, eliminating  $\bar{H}_{\text{dif}}$  reduces the ID by one unit to 7 and 8, respectively. This effect on the ID indicates that there are important asymmetries involving the environments of the two hydrogen atoms that can donate hydrogen bonds. A clear example of this is shown in Figure 1d, illustrating the creation of different types of topological defects.

**Free-Energy Landscape of Liquid Water.** Having computed the ID, we are now in a position to generate the high-dimensional free energies using the PAK-Nearest density estimator. One of the challenges in constructing the point-free energies is that the error grows with the ID.<sup>51</sup> We thus begin by focusing our analysis on using the SOAP descriptor environments consisting of only the oxygen atoms with a radial cutoff of 3.7 Å.

Visualizing the high-dimensional free energies is extremely challenging. With the PAK free energies, we performed the modified density peak clustering using a confidence interval of  $z = 2.5$ , which indicates the presence of one big cluster. The presence of one cluster at this  $z$  value is reproduced across several different water molecule environments, suggesting that this is not an artifact of statistical fluctuations.

In order to gain a more visual inspection of the free-energy landscape, we project the SOAP coordinates in two dimensions using the UMAP method.<sup>86</sup> Although reducing the dimensionality below the ID leads to an unavoidable information loss, the UMAP method has shown to fairly preserving the global structure of the data,<sup>89</sup> providing a convenient way to visualize the free energies. The left panel of Figure 3 shows the free-energy surface (FES) obtained with UMAP. Interestingly, the landscape is characterized by a very broad and rather flat free energy with small barriers ( $k_B T$ ) separating shallow minima. These minima are characterized by water environments that

are quite diverse, as seen in the three snapshots taken at various points in the basin. These fluctuations between defective and non-defective environments without deep minima are consistent with the presence of short-lived (between fs–ps) heterogeneities in water.<sup>25,37</sup> The right panel of Figure 3 shows a 2D-contour map along the UMAP coordinates colored by the free energy, which more clearly illustrates these features and confirms that at these temperatures, liquid water is indeed a homogeneous liquid.<sup>9,17</sup> The UMAP manifold for two other data sets corresponding to different choices of water molecule environments were found to be essentially the same, suggesting that the main features of the landscape are not artefacts of statistical fluctuations (see Figure S2).

The preceding analysis is performed on the SOAP descriptors involving only oxygen atoms within 3.7 Å. Since the ID changes quite significantly when including the hydrogen atoms, we repeated the PAK and UMAP analysis with the other SOAP variable combinations. Expanding the solvation environment does not lead to any significant changes in the free-energy landscape. More quantitatively, Figure S3 in the Supporting Information shows a scatter plot of the free energies comparing the results using  $\bar{O}$  and  $(\bar{O}, \bar{H}_{\text{ave}}, \bar{H}_{\text{dif}})$ , both with a radial cutoff 3.7 Å using the same water coordinates. The two free energies are very well correlated with each other and shows that while the hydrogen atoms expand the dimensionality of the free-energy landscape, the key physical features remain very similar. As pointed out earlier, the full descriptor including the hydrogens is important for distinguishing different defect environments, and therefore, the effects on the underlying free energy may become more pronounced in regimes where these defects are enhanced such as the air–water interface.<sup>65</sup>

The current results have been extracted using the TIP4P/2005 water model. To validate our results, we repeated our procedure of extracting the ID, PAK, and UMAP projection on trajectories of the MB-pol water model at room temperature.<sup>53</sup> In this model, we also observe the same features, namely, the

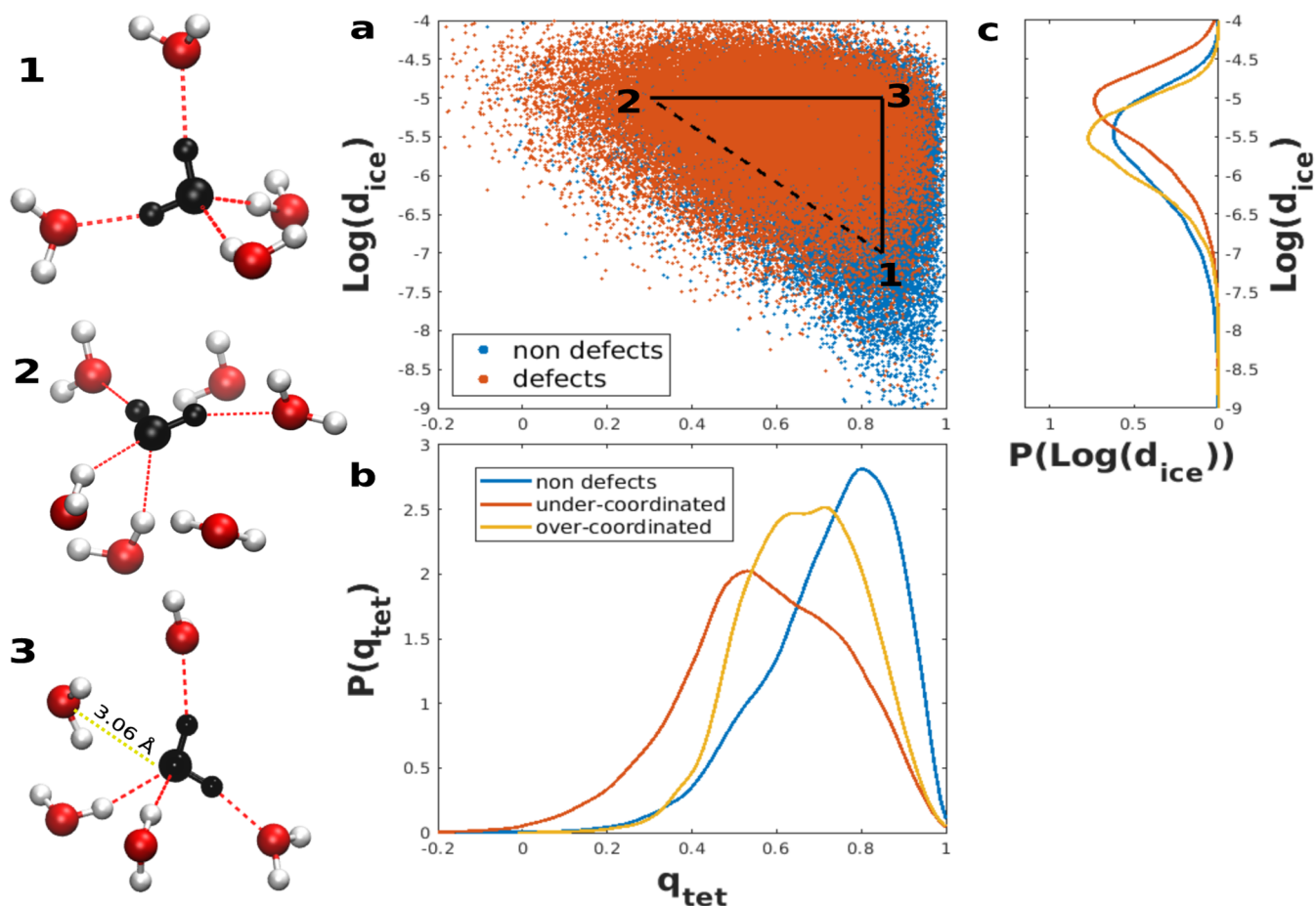


**Figure 4.** (a) Scatter plot of  $q_{tet}$  vs  $\text{Log}(d_{ice})$  with three points, which correspond to the environments shown on the left. The points are colored to differentiate between defects and non-defects. A large overlap is found between defects and non-defects. (b,c) Probability density distributions along  $q_{tet}$  and  $\text{Log}(d_{ice})$  for non-defects, and, under and over coordinated defects, as defined in the main text.

presence of a broad and flat free-energy landscape (see Supporting Information, Figure S4).

#### Molecular Origins of High-Dimensional Fluctuations.

The preceding analysis of the ID shows that the fluctuations involving the hydrogen bond network involve a rather larger number of solvent degrees of freedom moving in different directions. In the following, we will examine the correlations that exist between the various chemically inspired coordinates such as  $q_{tet}$ ,  $d_5$ , LSI, and Voronoi density ( $\rho_{vor}$ ), as well as the new SOAP-based descriptor,  $d_{ice}$ , that was described earlier. Note that in this analysis, a radial cutoff of 3.7 Å is used. Also in this discussion, we restrict our analysis to results in which  $d_{ice}$  was computed with only oxygen atoms. It is worth noting that the trends in behavior were found to be similar when the hydrogen atoms were included and when the radial cutoff was increased to 6.0 Å (see Figures S5 and S6).

**Tetrahedrality and  $d_{ice}$ .** We begin by showing in Figure 4 a scatter plot of  $q_{tet}$  and  $\text{Log}(d_{ice})$ . Also three points (1–3) are highlighted, which are illustrated top-down in the leftmost part of the figure. The  $q_{tet}$  and  $\text{Log}(d_{ice})$  values refer to that of the central water colored in black. The dashed line connecting points 1 and 2 corresponds to the regime where these two variables are strongly correlated with each other. Specifically, point 1 is a water environment that has a high tetrahedrality and a large negative value of  $\text{Log}(d_{ice})$ , implying that it is closer in distance to a locally ice-like environment. Point 2, on the other hand, has a low tetrahedrality and is non ice-like. The

origin of the difference between these two structures is seen more clearly in the image shown in point 2; there is an asymmetry in the angles between the donating and accepting side that are used to compute the tetrahedrality.

Perhaps the more surprising aspects of Figure 4 are all the points that lie above the dashed line. One of these limiting cases is shown by point 3, which has a high tetrahedrality but a large distance from ice using the SOAP coordinates. This environment illustrated by point 3 shows that there is a water molecule that is within the first shell ( $\sim 3.23$  Å) that is not hydrogen bonded to the central water. Nonetheless, the angles that are used to extract  $q_{tet}$  involving only the nearest four neighbors do not include this water molecule, and thus, the central water is flagged incorrectly as a tetrahedral environment.

Also shown in Figure 4 are the overlapped scatter plots for the defective and non-defect water molecules. Recall that defect waters are those which break the ice rules of accepting and donating two hydrogen bonds. Figure 4b,c shows the 1D distributions for  $\text{Log}(d_{ice})$  and  $q_{tet}$  for non-defects, under-coordinated (defined as when the sum of the number of donating and accepting hydrogen bonds is less than 4) and over-coordinated defects (where the sum of the number of donating and accepting hydrogen bonds is greater than 4). In this case, we see that while  $q_{tet}$  and  $\text{Log}(d_{ice})$  are both characterized by differences in their average values for defect



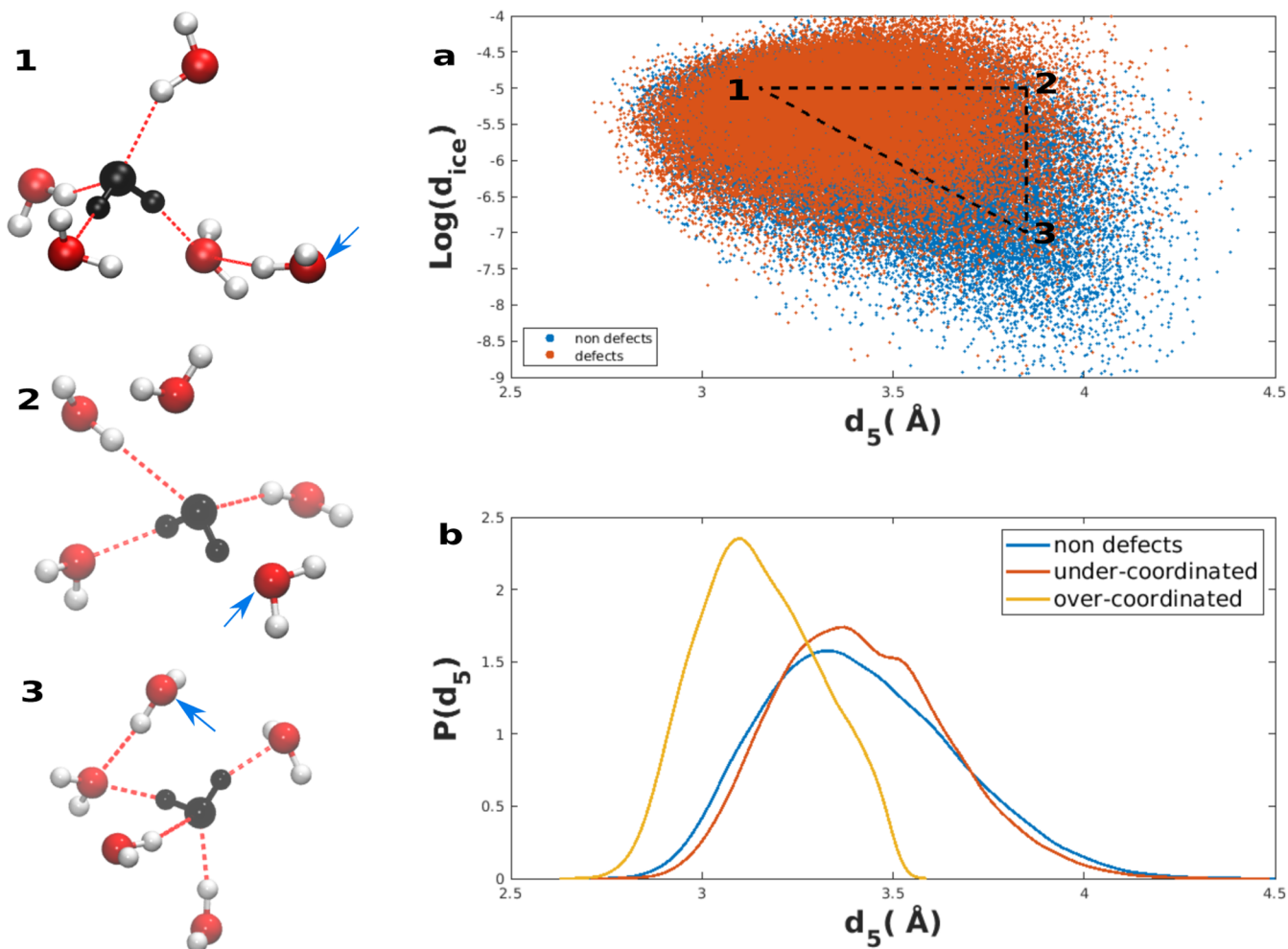


**Figure 5.** (a) Scatter plot of  $d_5$  vs  $\text{Log}(d_{\text{ice}})$  with the three numbered configurations corresponding to the environments shown pictorially on the left. The blue arrow points to the water molecule that satisfies the  $d_5$ th criterion. (b) Probability densities obtained along  $d_5$  for the defective and non-defective water molecules.

and non-defect populations, the former appears to show larger variation across the different environments.

**$d_5$  and  $d_{\text{ice}}$ .** Figure 5 shows the analysis performed on  $d_5$  and  $\text{Log}(d_{\text{ice}})$ . The  $d_5$  parameter was designed in order to quantify fluctuations that occur between the first and second hydration shell.<sup>31</sup> Specifically, a larger  $d_5$  has been interpreted as a water environment that is more open and low-density like, whereas smaller values of  $d_5$  are shown as compact and high-density like.

Similar to that analysis, we illustrate three landmark points in the scatter plot which are illustrated to the left of Figure 5. The water molecules referred to by the blue arrow correspond to waters that satisfy the  $d_5$ th criterion. The fluctuations along the line connecting points 1 and 3 reflect changes where the two parameters are well correlated: point 1 is a locally tetrahedral environment where the  $d_5$  water resides in the second shell and separated by two hydrogen bonds from the central water, while in point 3, the  $d_5$  water undergoes a large fluctuation bringing it from 3.7 Å to within 3.1 Å of the central water.

The fluctuations along the points 1–2 and 2–3 are more non-trivial as it shows that both  $d_{\text{ice}}$  and  $d_5$  play an important role in characterizing the local environments independently. Although point 2 has a high  $d_5$  of approximately 3.7 Å, asymmetries in the hydrogen bonds between the donating and accepting side of the first shell render it with a local

configuration that is non-ice like. Examining the constrained distributions of the  $d_5$  for the non-defects and under/over coordinated defects as before shows that unlike  $q_{\text{tet}}$   $d_5$  is much less sensitive in distinguishing these different environments. Intuitively, this is because the  $q_{\text{tet}}$  is a parameter that uses the four nearest neighbors, whereas  $d_5$  focuses on just a single water molecule that fluctuates between the first and second hydration shell.

**Voronoi Density( $\rho$ ) and  $d_{\text{ice}}$ .** Figure 6 shows the analysis performed on the Voronoi density  $\rho$  and  $\text{Log}(d_{\text{ice}})$ . The  $\rho$  parameter has been used previously in the literature<sup>10,25,38</sup> to quantify local density fluctuations in liquid water at different thermodynamic conditions. As carried out in the previous analysis, a series of landmark points are illustrated to aid with the discussion. The fluctuations along the line connecting points 1 and 2 reflect changes where the two parameters are well correlated: point 1 is a low density open and ice-like environment, whereas point 2 corresponds to a higher-density environment with eight neighboring waters within 3.7 Å. As expected, this high-density fluctuation leads to the creation of an environment with a low value of  $\text{Log}(d_{\text{ice}})$ .

Moving along points 1–3 and 2–3 confirms again the importance of understanding the fluctuations of the network using a combination of several different variables. Point 2 is a high-density environment created by a water molecule that



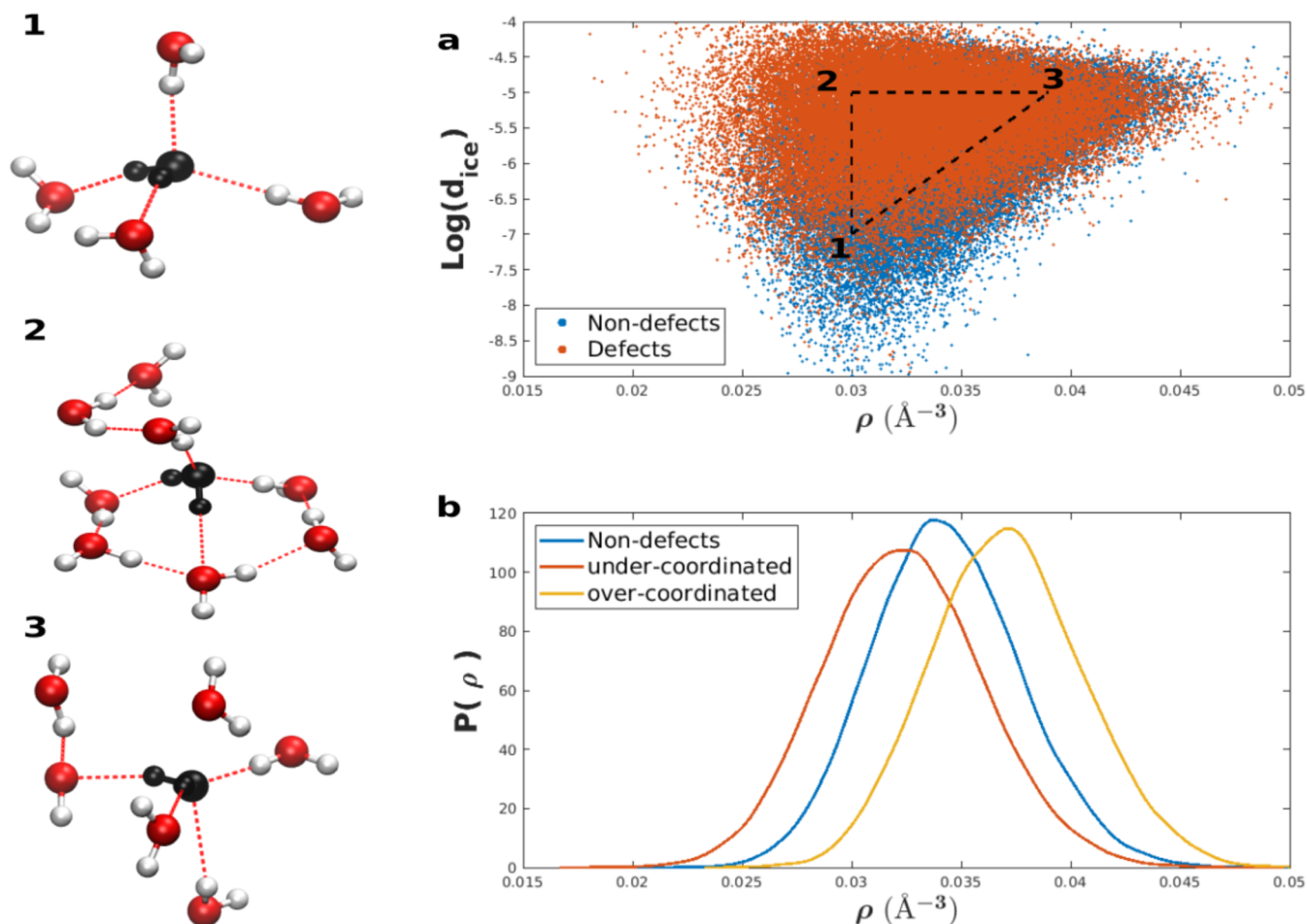


**Figure 6.** (a) Scatter plot of  $\rho$  vs  $\text{Log}(d_{\text{ice}})$  with the three-numbered configurations corresponding to the environments shown pictorially on the left. (b) Probability densities obtained along  $\rho$  for the defective and non-defective water molecules.

participates in a six-membered ring and maintains a local tetrahedral order and therefore has a low value of  $\text{Log}(d_{\text{ice}})$ . Point 3, on the other hand, corresponds to a low-density environment, but the orientations of the nearby water molecules do not have a local tetrahedral structure, therefore leading to a higher value of  $\text{Log}(d_{\text{ice}})$ . Figure 6c shows the  $\rho$  parameter performs rather well compared to the  $d_5$  at distinguishing over and undercoordinated defect water molecules. It is interesting to note, however, that there is significant overlap in the densities for water molecules that accept and donate 2 hydrogen bonds and both under/over coordinated waters.

**LSI and  $d_{\text{ice}}$ .** Finally, we conclude this section with a comparison of the LSI- and SOAP-based parameter  $d_{\text{ice}}$  (Figure 7). The LSI variable was designed in order to quantify fluctuations between more ordered and disordered environments due to fluctuations at the boundary between the first and the second solvation shell.<sup>30,90</sup> Specifically, a larger value of LSI has been interpreted as a water environment that is more open and characterized by a separation between the first and the second shell, whereas smaller values of LSI correspond to environments without a well-separated first and second shell, owing to the presence of interstitial waters.

The dashed line connecting points 1 and 3 corresponds to the regime where these two variables are well correlated with each other. Specifically, point 1 is a water environment that has a large LSI and a large negative value of  $\text{Log}(d_{\text{ice}})$ , implying

that it looks locally like an ice-like environment. Point 3, on the other hand, has a low LSI and is non-ice like. The origins of the difference between these two structures is seen more clearly in the leftmost panels where we observe in point 3 the presence of several interstitial water molecules.

The region connecting the points 2 and 3 illustrates the challenge in interpreting the LSI coordinate in terms of the local order/disorder. Point 2, which has a small distance from ice, but smaller separation between first and second shell is found to have the same LSI value as point 3 which corresponds to a rather compressed and high-density unicy environment. Although the effect is subtle, the LSI does better at separating undercoordinated waters from those that are overcoordinated which look very similar to non-defective waters.

#### Evolution of Molecular Descriptors with Free Energy.

In the preceding sections, we have shown that the free-energy landscape of liquid water at room temperature is best characterized as having one broad basin with small barriers separating the different minima. Furthermore, we have also seen, as anticipated by ID analysis, that the fluctuations within this landscape involve the coupling of several different molecular descriptors. In this section, we explore how these quantities change as a function of the free energy at room temperature. In addition, we also examine the behavior of some of the descriptors close to the critical point of supercooled water based on an analysis of microsecond long trajectories by Debenedetti and Sciortino.<sup>20</sup>

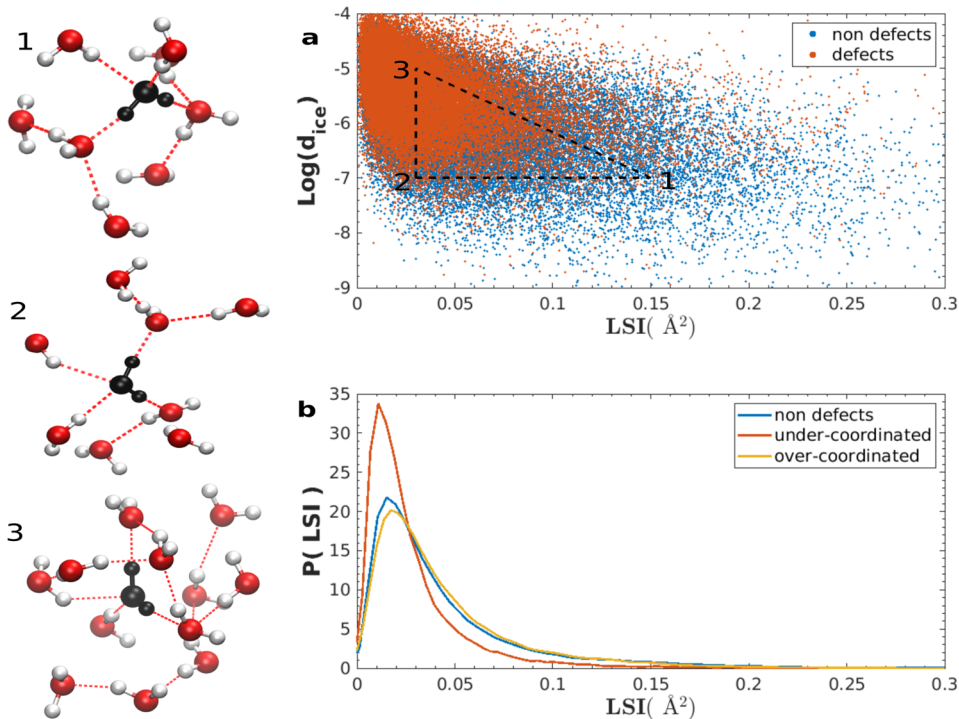


**Figure 7.** (a) Scatter plot of LSI vs  $\text{Log}(d_{\text{ice}})$  with the three-numbered configurations corresponding to the environments shown pictorially on the left. (b) Probability densities obtained along the LSI for the defective and non-defective water molecules.

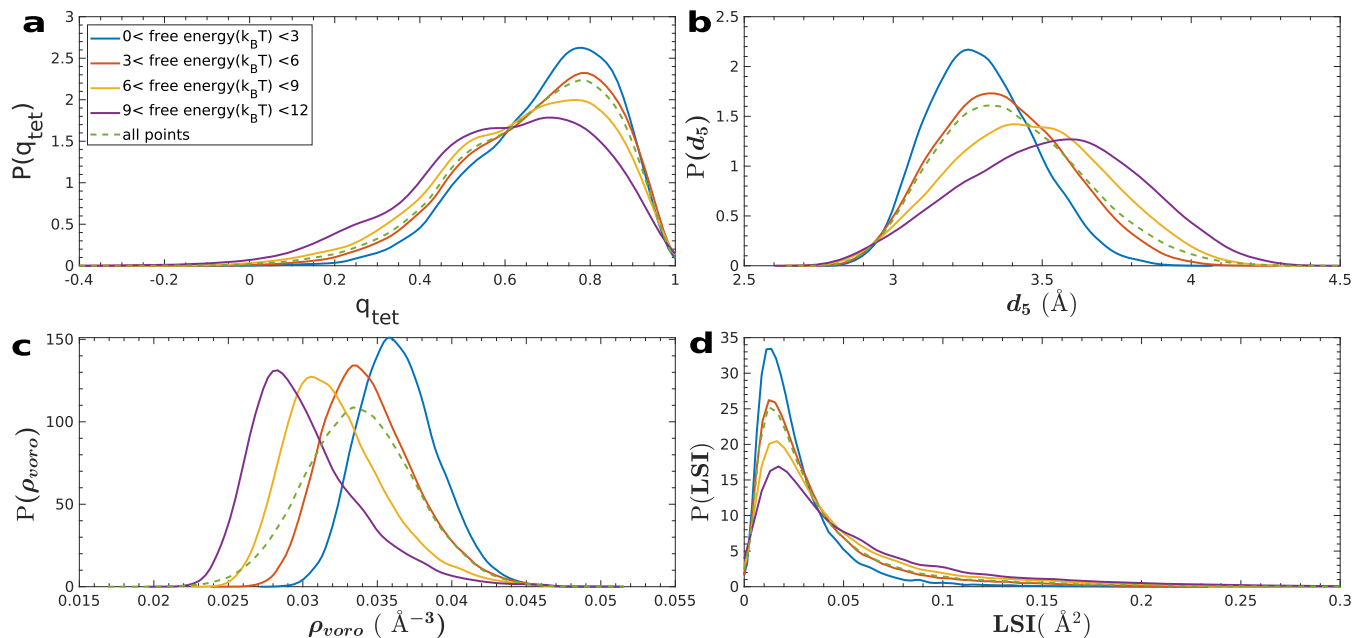


**Figure 8.** (a–d) Evolution of the chemical-based parameters as a function of different cuts along the free energy (as shown with the various colored curves). The dashed curve in each panel corresponds to the distribution obtained by averaging over all the water molecules regardless of its free energy.

**Room-Temperature Liquid Water.** Using the free energies of the points extracted earlier, we examined how the various descriptors, evolve as a function of being on different regions of the FES. **Figures 8** and **9** show distributions of  $q_{\text{tet}}$ ,  $d_5$ , LSI,  $\rho_{\text{voro}}$  and  $\text{Log}(d_{\text{ice}})$  in slices of the free energy, ranging between the minimum and  $10 k_{\text{B}}T$ . Also shown in each panel is the distribution of the respective variable obtained from all points independent of its position on the FES.

Starting with  $q_{\text{tet}}$  we observe that the water tetrahedrality reduces as one moves higher in FES. Interestingly, the shoulder at lower values of  $q_{\text{tet}} \sim 0.5$  becomes much more pronounced for the points higher up in the FES and is consistent with the creation of more defects (see Supporting Information, **Figure S7**). The evolution of the variables such as  $d_5$  and  $\rho_{\text{voro}}$  reflect other changes in the hydrogen bond network. In particular,  $d_5$  increases from 3.3 to 3.5 Å moving above the minimum in free energy, whereas  $\rho_{\text{voro}}$  decreases from 0.037 to 0.03 Å<sup>-3</sup>. These

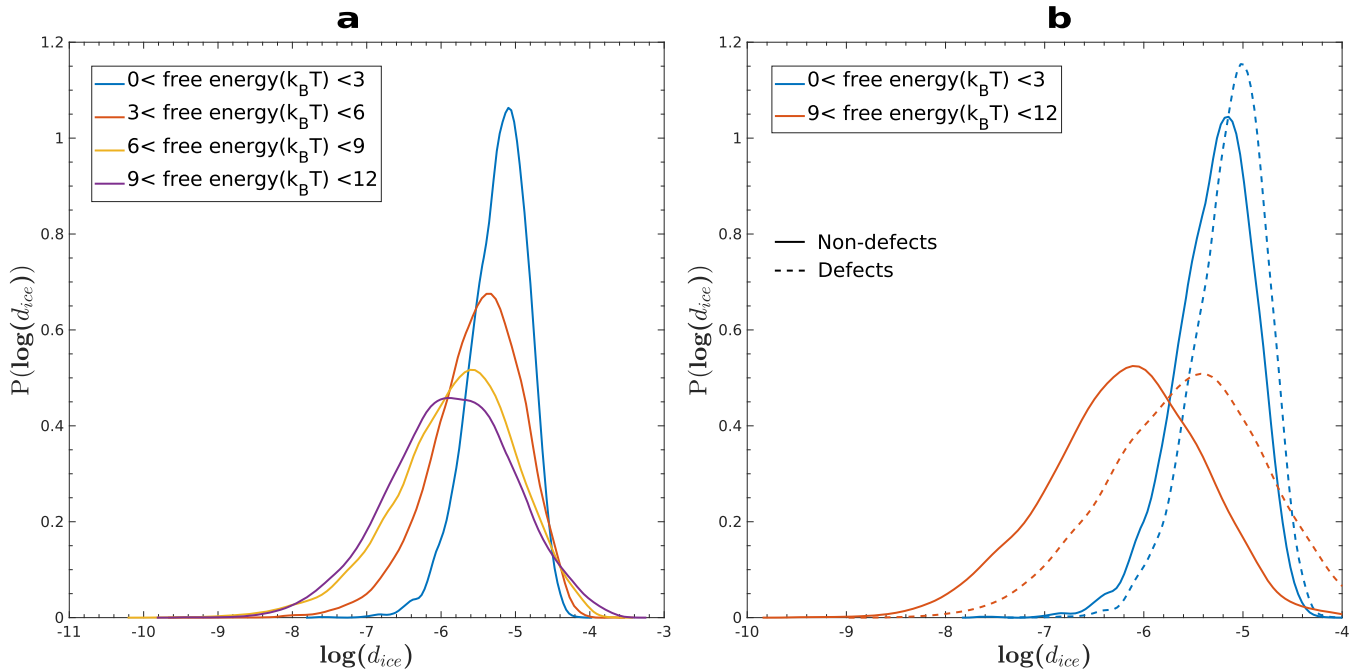


**Figure 9.** (a) Evolution of  $\text{Log}(d_{ice})$  as a function of different free-energy cuts. (b)  $\text{Log}(d_{ice})$  for a low and high free-energy region specifically for defective and non-defective water.

changes correspond to water environments that become more open and less tetrahedral. It is also worth noting that the points near the minima correspond to densities that are 12% larger than the average bulk density. The LSI distributions in Figure 8d show more subtle changes toward higher values as a function of free energy again consistent with the formation of a more open local structure. It is clear however that there is significant overlap along all these variables across the entire free-energy landscape.

The left panel of Figure 9 shows the distributions of  $\text{Log}(d_{ice})$  for different free-energy cuts. Interestingly, as one moves to regions of the FES that are higher in free energy, the environments look more ice-like which is consistent with the lower free-energy structures in ambient temperature water, being dominated by high density and more disordered environments. In the right panel of Figure 9, the changes in  $\text{Log}(d_{ice})$  as a function of free energy for both defective and non-defective water molecules are shown. First, we note that the free-energy minimum is characterized by the presence of both defective and non-defective water molecules, consistent with the earlier analysis on the presence of a broad free-energy basin characterized by low barriers separating different water structures. Second, we observe that fluctuations in the hydrogen bond network away from the free-energy minimum result in the creation of both more ice-like or less-ice like environments, as revealed by the changes in  $\text{Log}(d_{ice})$ . For non-defects which accept and donate two hydrogen bonds, the higher lying free-energy structures arise from more-ice like environments, which are energetically stabilized but entropically disfavored.

Although the  $\text{Log}(d_{ice})$  we have used in this analysis only uses the oxygen atoms, we have shown earlier that the inclusion of the hydrogen atoms contains important information, as shown by ID (see Figure 2) and SOAP-distance analysis (see Supporting Information, Figure S1). To see this a bit better within the context of  $d_{ice}$ , we compared the

distribution of  $\text{Log}(d_{ice})$  for defects and non-defects comparing  $\vec{O}$ ,  $(\vec{O}, \vec{H}_{ave})$ , and  $(\vec{O}, \vec{H}_{ave}, \vec{H}_{dif})$ . This analysis shows that when information of the environments of hydrogen atoms is included,  $\text{Log}(d_{ice})$  differentiates better between defects and non-defects (see Figures S8 and S9).

As alluded to earlier, recent theoretical studies proposed the possibility of fused dodecahedron structures as a possible source of a low-density environment in water.<sup>72</sup> In order to assess this possibility, we also examined the  $d_{dod}$  distance, as described in the methods section. In the models of liquid water examined in this work, the environments in room-temperature water yield larger values for  $d_{dod}$  compared to  $d_{ice}$  (see Figure S10).

All in all, we see that the free-energy landscape of water is best thought of as a broad and rather flat free-energy landscape characterized by both defective and non-defective water molecules. Moving up higher in free energy from this broad minimum can result in the creation of both more tetrahedral or non-tetrahedral and defective water molecules. In this context, fluctuations between different species involve the competition between both entropic and enthalpic terms that compensate each other. Breaking a hydrogen bond from a water molecule, that accepts and donates two hydrogen bonds to create a defect that either accepts or donates only one hydrogen bond, will roughly incur an energetic cost of approximately  $5k_B T$ . However, this would be entropically driven by a  $T\Delta S$  term equivalent to about  $10k_B T$  to yield a positive change in free energy of  $5k_B T$ . On the other hand, one can also move higher in free energy beginning to create more ordered tetrahedral environments. While this is enthalpically favored, it incurs an entropic penalty. Dissecting these contributions as a function of temperature would be an interesting subject of study in future.

**Supercooled Liquid Water.** In a recent work, the second critical point of water was studied from long microsecond simulations of realistic point-charge water models.<sup>20</sup> In these



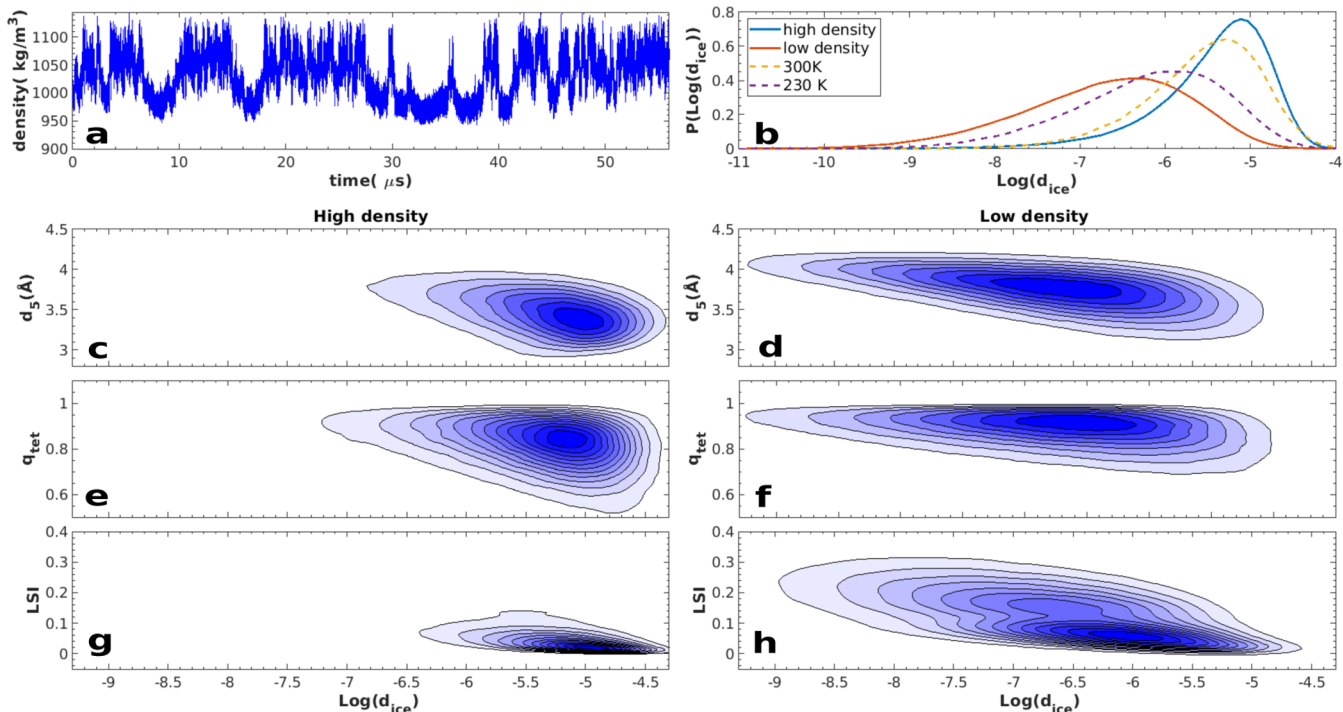


**Figure 10.** (a) Plot of the time series of the global density of the trajectory at 171 K, 1751 bars. (b) Comparison of the  $\text{Log}(d_{\text{ice}})$  at 3.7 Å between environments in HD and LD regions contrasted with  $\text{Log}(d_{\text{ice}})$  at 230 and 300 K. (c–h) 2D kernel density estimates of the  $\text{Log}(d_{\text{ice}})$  vs chemical-based parameters. (c,d) Plots  $d_5$  and  $\text{Log}(d_{\text{ice}})$  for HD and LD regions, respectively. (e,f)  $q_{\text{tet}}$  and  $\text{Log}(d_{\text{ice}})$ . (g,h) Plots LSI and  $\text{Log}(d_{\text{ice}})$ . The growth of a shoulder is observed in the LD phase for that the LSI.

simulations close to the critical point of water at  $\sim 171$  K, 1751 bars, fluctuations between a high-density (HD) phase at  $1064 \text{ kg m}^{-3}$  and a low-density (LD) phase at  $977 \text{ kg m}^{-3}$  were observed. These transitions occurring over the course of several 10 s of microseconds are illustrated in Figure 10a. The local water environments of the HD and LD phases have typically been rationalized using chemical-based descriptors such as  $q_{\text{tet}}$ , LSI, and the bond-order Steinhardt order parameters.<sup>5,12,15,19,30,31,91</sup>

We have seen earlier that a combination of the chemical-based parameters and SOAP variables provides a more nuanced perspective on the nature of the fluctuations in the hydrogen bonded network. In Figure 10b, we show the  $\text{Log}(d_{\text{ice}})$  distributions for water environments extracted from the HD and LD regions of the trajectory in panel (a). Specifically, SOAP environments were determined for all water in the frames where the density was within  $1 \text{ kg m}^{-3}$  of the minimum in the HD phase and LD phase separately. Additionally, the distributions for water at 300 K and supercooled water at 230 K are also shown. The LD phase is characterized by water environments that are more ice-like by 4–5 orders of magnitude compared to those in the HD phase. As expected, the environments observed in bulk water at 300 K are much more similar to those in the HD phase close to the critical point. Interestingly, even though the global densities are quite different, there is a significant region of overlap in the environments observed in the HD and LD phases. This suggests the existence of heterogeneities within each of the liquid phases at the critical point.

Figure 10c–h shows the behavior of the coupling between the  $d_5$ ,  $q_{\text{tet}}$  and LSI parameters as a function of  $\text{Log}(d_{\text{ice}})$  for the HD and LD phases in the left and right panels, respectively. For both  $d_5$  and  $q_{\text{tet}}$  in panels (c–f), the extent of the

correlation between these variables and  $\text{Log}(d_{\text{ice}})$  changes rather significantly when comparing the HD and LD phases. For the LD phase, there appear to be a significant number of environments that have a large  $d_5$  and high tetrahedrality but cover a broad spread of  $\text{Log}(d_{\text{ice}})$  values. The LSI for the LD phase is the only variable that shows the presence of a bimodal character. However in the HD phase, most of the local environments have the signatures of a closed, non-tetrahedral, and higher local density (see Supporting Information, Voronoi Figure S11). A visual inspection of the trajectories suggests that the LD phase is characterized by the presence of larger domains that are built up of both low (where there are connected regions with lower  $d_{\text{ice}}$ ) and smaller intermediately high-density regions (with larger values of  $d_{\text{ice}}$ ). Details of this analysis will be the subject of a forthcoming study.<sup>92</sup>

## CONCLUSIONS

There is currently tremendous growth in the development and application of machine learning methods to understand the complex molecular systems. These approaches are aimed at circumventing the intervention of human or chemical bias and allowing for helping interpreting the physical models that are beyond chemical imagination.

In this work, we have used a series of advanced unsupervised learning techniques to study the fluctuations in simulated liquid water at room temperature. This procedure involves the use of state-of-the-art local atomic descriptors (SOAP) to describe the water environments, followed by the extraction of the ID of the water network and then finally determining the topography of the free-energy landscape. We also complement this analysis by studying the behavior of various chemically inspired coordinates that have been used to study water structure. We believe that this establishes a rigorous theoretical

protocol for studying fluctuations in liquids and aqueous solutions in general.

The unsupervised learning techniques we have used serves as a step toward solving the conflicting results regarding the question on whether liquid water is a homogeneous or heterogeneous liquid which arise from analyzing the water environment appearing in a simulation with different human-defined collective variables. However, it should be stressed that the unsupervised approach does not fully remove the analysis biases and, hence, it does not provide a definite solution to the problem. Among the possible sources of error, one should consider that there are several alternatives when choosing the high-dimensional representation of the environments and the analysis methods, so one cannot discard that a different choice leads to different results.

Moreover, these methods are not parameter-free, so the selection of the parameters will also introduce some errors. Finally, the interpretation of our supervised learning protocol results has been carried out using a set of collective variables, which will also introduce some bias. Having said all this, it should be stressed that one important take-home message of this work is that the combination of both unsupervised and chemical-intuition-based parameters provide a more nuanced description on the thermodynamic landscape of liquid water.

Our analysis confirms previous several theoretical and experimental observations that room-temperature water is a homogeneous liquid. However, the picture that emerges is much more nuanced. Fluctuations in the hydrogen bond network occur on a rather high-dimensional free-energy landscape that is broad and rather flat with small ripples separated by small free-energy barriers. These features are found both in TIP4P/2005 water and in the many-body potential MB-pol water.<sup>53</sup> This implies the presence of short-lived heterogeneities on the fs-to-ps timescale. The use of SOAP descriptors, by revealing the intrinsically multidimensional character of the local environment, leads to an additional conclusion: individually, variables such as  $q_{\text{tet}}$ ,  $d_5$ , LSI, or for that matter  $d_{\text{ice}}$ , cannot be used to infer the existence of LDL- or HDL-like environments.

Finally, we also explore the evolution of all these variables within the supercooled regime by analyzing trajectories from recent work by Sciortino and Debenedetti.<sup>20</sup> While the HDL phase in supercooled water resembles the majority of local water environments in room-temperature water, the situation is more complicated with LDL. Here, there appear to be larger domains involving water environments that are more ice-like and high-density-like but lower than the density of the HDL phase. The possibility of creating these domains is consistent with an earlier study by some of us showing that upon supercooling, a network of connected branched voids develop surrounded by smaller spherical cavities.<sup>40</sup> Work is underway to apply the unsupervised learning approaches to characterize the free-energy landscape of water near the critical point and will be subject of future work.

## ■ ASSOCIATED CONTENT

### SI Supporting Information

The Supporting Information is available free of charge at <https://pubs.acs.org/doi/10.1021/acs.jctc.1c01292>.

Sensitivity of our analysis for inclusion of hydrogen atoms, second shell effects, different choices of molecule environments, and different water model (MB-pol);  $q_{\text{tet}}$

of defective/non-defective environments at high free energies; and  $\text{Log}(d_{\text{ice}})$  and  $\text{Log}(d_{\text{dod}})$  and 2D density plots of  $\text{Log}(d_{\text{ice}})$  vs  $\rho_{\text{voro}}$  for HDL and LDL environments (PDF)

## ■ AUTHOR INFORMATION

### Corresponding Authors

Ali Hassanali — *The Abdus Salam International Center for Theoretical Physics, 34151 Trieste, Italy*; [orcid.org/0000-0002-3208-1488](https://orcid.org/0000-0002-3208-1488); Email: [ahassana@ictp.it](mailto:ahassana@ictp.it)

Alex Rodriguez — *The Abdus Salam International Center for Theoretical Physics, 34151 Trieste, Italy*; Email: [alexdepremia@gmail.com](mailto:alexdepremia@gmail.com)

### Author

Adu Offei-Danso — *The Abdus Salam International Center for Theoretical Physics, 34151 Trieste, Italy*; SISSA—International School for Advanced Studies, 34136 Trieste, Italy; [orcid.org/0000-0002-8035-0769](https://orcid.org/0000-0002-8035-0769)

Complete contact information is available at: <https://pubs.acs.org/10.1021/acs.jctc.1c01292>

### Notes

The authors declare no competing financial interest.

## ■ ACKNOWLEDGMENTS

The authors acknowledge Francesco Paesani for sharing trajectories of MB-pol water and Francesco Sciortino for sharing the supercooled water trajectories of TIP4P/2005.

## ■ REFERENCES

- (1) Franks, F. *Water: A Matrix of Life*; Royal Society of Chemistry, 2000; Vol. 21.
- (2) Ball, P. Water as an active constituent in cell biology. *Chem. Rev.* **2008**, *108*, 74–108.
- (3) Evans, M. W.; Robinson, G. W.; Singh, S.; Zhu, S.-b. *Water in Biology, Chemistry and Physics: Experimental Overviews and Computational Methodologies*; World Scientific, 1996; Vol. 9.
- (4) Chaplin, M. F. Structure and properties of water in its various states. *Encyclopedia of Water: Science, Technology, and Society*; Wiley, 2019; pp 1–19.
- (5) Debenedetti, P. G. Supercooled and glassy water. *J. Phys.: Condens. Matter* **2003**, *15*, R1669.
- (6) Angell, C. A. Amorphous water. *Annu. Rev. Phys. Chem.* **2004**, *55*, 559–583.
- (7) Smith, J. D.; Cappa, C. D.; Wilson, K. R.; Messer, B. M.; Cohen, R. C.; Saykally, R. J. Energetics of hydrogen bond network rearrangements in liquid water. *Science* **2004**, *306*, 851–853.
- (8) Geiger, A.; Stanley, H. E. Low-Density “Patches” in the Hydrogen-Bond Network of Liquid Water: Evidence from Molecular-Dynamics Computer Simulations. *Phys. Rev. Lett.* **1982**, *49*, 1749.
- (9) Duboué-Dijon, E.; Laage, D. Characterization of the Local Structure in Liquid Water by Various Order Parameters. *J. Phys. Chem. B* **2015**, *119*, 8406–8418.
- (10) Yeh, Y.-I.; Mou, C.-Y. Orientational relaxation dynamics of liquid water studied by molecular dynamics simulation. *J. Phys. Chem. B* **1999**, *103*, 3699–3705.
- (11) Rao, F.; Garrett-Roe, S.; Hamm, P. Structural inhomogeneity of water by complex network analysis. *J. Phys. Chem. B* **2010**, *114*, 15598–15604.
- (12) Holten, V.; Palmer, J. C.; Poole, P. H.; Debenedetti, P. G.; Anisimov, M. A. Two-state thermodynamics of the ST2 model for supercooled water. *J. Chem. Phys.* **2014**, *140*, 104502.
- (13) Röntgen, W. C. Ueber die Constitution des flüssigen Wassers. *Ann. Phys.* **1892**, *281*, 91–97.

- (14) Nilsson, A.; Huang, C.; Pettersson, L. G. M. Fluctuations in ambient water. *J. Mol. Liq.* **2012**, *176*, 2–16.
- (15) Taschin, A.; Bartolini, P.; Eramo, R.; Righini, R.; Torre, R. Evidence of two distinct local structures of water from ambient to supercooled conditions. *Nat. Commun.* **2013**, *4*, 2401.
- (16) Wernet, P.; Nordlund, D.; Bergmann, U.; Cavalleri, M.; Odellius, M.; Ogasawara, H.; Näslund, L. A.; Hirsch, T. K.; Ojamäe, L.; Glatzel, P.; et al. The structure of the first coordination shell in liquid water. *Science* **2004**, *304*, 995–999.
- (17) Soper, A. K. Is water one liquid or two? *J. Chem. Phys.* **2019**, *150*, 234503.
- (18) Pettersson, L. G. A. Two-State Picture of Water and the Funnel of Life. *International Conference Physics of Liquid Matter: Modern Problems*; Springer, 2018; pp 3–39.
- (19) Gallo, P.; Amann-Winkel, K.; Angell, C. A.; Anisimov, M. A.; Caupin, F.; Chakravarty, C.; Lascaris, E.; Loerting, T.; Panagiotopoulos, A. Z.; Russo, J.; et al. Water: A tale of two liquids. *Chem. Rev.* **2016**, *116*, 7463–7500.
- (20) Debenedetti, P. G.; Sciortino, F.; Zerze, G. H. Second critical point in two realistic models of water. *Science* **2020**, *369*, 289–292.
- (21) Gartner, T. E.; Zhang, L.; Piaggi, P. M.; Car, R.; Panagiotopoulos, A. Z.; Debenedetti, P. G. Signatures of a liquid-liquid transition in an ab initio deep neural network model for water. *Proc. Natl. Acad. Sci.* **2020**, *117*, 26040–26046.
- (22) Accordino, S.; Fris, J. R.; Sciortino, F.; Appignanesi, G. Quantitative investigation of the two-state picture for water in the normal liquid and the supercooled regime. *Eur. Phys. J. E* **2011**, *34*, 48.
- (23) Wikfeldt, K. T.; Nilsson, A.; Pettersson, L. G. M. Spatially inhomogeneous bimodal inherent structure of simulated liquid water. *Phys. Chem. Chem. Phys.* **2011**, *13*, 19918–19924.
- (24) Myneni, S.; Luo, Y.; Näslund, L. Å.; Cavalleri, M.; Ojamäe, L.; Ogasawara, H.; Pelmenchikov, A.; Wernet, P.; Väterlein, P.; Heske, C.; et al. Spectroscopic probing of local hydrogen-bonding structures in liquid water. *J. Phys.: Condens. Matter* **2002**, *14*, L213.
- (25) Stirnemann, G.; Laage, D. Communication: On the Origin of the Non-Arrhenius Behavior in Water Reorientation Dynamics. *J. Chem. Phys.* **2012**, *137*, 031101.
- (26) Henchman, R. H. Water's dual nature and its continuously changing hydrogen bonds. *J. Phys.: Condens. Matter* **2016**, *28*, 384001.
- (27) Kühne, T. D.; Khaliullin, R. Z. Electronic signature of the instantaneous asymmetry in the first coordination shell of liquid water. *Nat. Commun.* **2013**, *4*, 1450.
- (28) Giovambattista, N.; Debenedetti, P. G.; Sciortino, F.; Stanley, H. E. Structural order in glassy water. *Phys. Rev. E: Stat., Nonlinear, Soft Matter Phys.* **2005**, *71*, 061505.
- (29) Yan, Z.; Buldyrev, S. V.; Kumar, P.; Giovambattista, N.; Debenedetti, P. G.; Stanley, H. E. Structure of the first- and second-neighbor shells of simulated water: Quantitative relation to translational and orientational order. *Phys. Rev. E: Stat., Nonlinear, Soft Matter Phys.* **2007**, *76*, 051201.
- (30) Appignanesi, G. A.; Rodriguez Fris, J. A.; Sciortino, F. Evidence of a two-state picture for supercooled water and its connections with glassy dynamics. *Eur. Phys. J. E* **2009**, *29*, 305–310.
- (31) Cuthbertson, M. J.; Poole, P. H. Mixture-like behavior near a liquid-liquid phase transition in simulations of supercooled water. *Phys. Rev. Lett.* **2011**, *106*, 115706.
- (32) Tanaka, H.; Tong, H.; Shi, R.; Russo, J. Revealing key structural features hidden in liquids and glasses. *Nat. Rev. Phys.* **2019**, *1*, 333–348.
- (33) Saika-Voivod, I.; Sciortino, F.; Poole, P. H. Computer simulations of liquid silica: Equation of state and liquid-liquid phase transition. *Phys. Rev. E: Stat. Phys., Plasmas, Fluids, Relat. Interdiscip. Top.* **2000**, *63*, 011202.
- (34) Gasparotto, P.; Hassanali, A. A.; Ceriotti, M. Probing defects and correlations in the hydrogen-bond network of ab initio water. *J. Chem. Theor. Comput.* **2016**, *12*, 1953–1964.
- (35) Agmon, N. Liquid water: From symmetry distortions to diffusive motion. *Acc. Chem. Res.* **2012**, *45*, 63–73.
- (36) Sciortino, F.; Fornili, S. L. Hydrogen bond cooperativity in simulated water: Time dependence analysis of pair interactions. *J. Chem. Phys.* **1989**, *90*, 2786–2792.
- (37) Henchman, R. H.; Irudayam, S. J. Topological hydrogen-bond definition to characterize the structure and dynamics of liquid water. *J. Phys. Chem. B* **2010**, *114*, 16792–16810.
- (38) Bernal, J. D. A geometrical approach to the structure of liquids. *Nature* **1959**, *183*, 141–147.
- (39) Ansari, N.; Dandekar, R.; Caravati, S.; Sosso, G. C.; Hassanali, A. High and low density patches in simulated liquid water. *J. Chem. Phys.* **2018**, *149*, 204507.
- (40) Ansari, N.; Laio, A.; Hassanali, A. Spontaneously forming dendritic voids in liquid water can host small polymers. *J. Phys. Chem. Lett.* **2019**, *10*, 5585–5591.
- (41) Ansari, N.; Onat, B.; Sosso, G. C.; Hassanali, A. Insights into the Emerging Networks of Voids in Simulated Supercooled Water. *J. Phys. Chem. B* **2020**, *124*, 2180–2190 PMID: 32032486.
- (42) Abascal, J. L. F.; Vega, C. A general purpose model for the condensed phases of water: TIP4P/2005. *J. Chem. Phys.* **2005**, *123*, 234505.
- (43) Bartók, A. P.; Kondor, R.; Csányi, G. On representing chemical environments. *Phys. Rev. B* **2013**, *87*, 184115.
- (44) Monserrat, B.; Brandenburg, J. G.; Engel, E. A.; Cheng, B. Liquid water contains the building blocks of diverse ice phases. *Nat. Commun.* **2020**, *11*, 5757.
- (45) Facco, E.; d'Errico, M.; Rodriguez, A.; Laio, A. Estimating the intrinsic dimension of datasets by a minimal neighborhood information. *Sci. Rep.* **2017**, *7*, 12140–8.
- (46) Jong, K.; Hassanali, A. A. A data science approach to understanding water networks around biomolecules: the case of tri-alanine in liquid water. *J. Phys. Chem. B* **2018**, *122*, 7895–7906.
- (47) Sormani, G.; Rodriguez, A.; Laio, A. Explicit Characterization of the Free-Energy Landscape of a Protein in the Space of All Its C $\alpha$  Carbons. *J. Chem. Theor. Comput.* **2019**, *16*, 80–87.
- (48) Mendes-Santos, T.; Turkeshi, X.; Dalmonte, M.; Rodriguez, A. Unsupervised learning universal critical behavior via the intrinsic dimension. *Phys. Rev. X* **2021**, *11*, 011040.
- (49) Mendes-Santos, T.; Angelone, A.; Rodriguez, A.; Fazio, R.; Dalmonte, M. Intrinsic Dimension of Path Integrals: Data-Mining Quantum Criticality and Emergent Simplicity. *PRX Quantum* **2021**, *2*, 030332.
- (50) Rodriguez, A.; Laio, A. Clustering by fast search and find of density peaks. *science* **2014**, *344*, 1492–1496.
- (51) Rodriguez, A.; d'Errico, M.; Facco, E.; Laio, A. Computing the free energy without collective variables. *J. Chem. Theor. Comput.* **2018**, *14*, 1206–1215.
- (52) d'Errico, M.; Facco, E.; Laio, A.; Rodriguez, A. Automatic topography of high-dimensional data sets by non-parametric Density Peak clustering. *Inf. Sci.* **2021**, *560*, 476 arXiv preprint arXiv:1802.10549.
- (53) Reddy, S. K.; Straight, S. C.; Bajaj, P.; Huy Pham, C.; Riera, M.; Moberg, D. R.; Morales, M. A.; Knight, C.; Götz, A. W.; Paesani, F. On the accuracy of the MB-pol many-body potential for water: Interaction energies, vibrational frequencies, and classical thermodynamic and dynamical properties from clusters to liquid water and ice. *J. Chem. Phys.* **2016**, *145*, 194504.
- (54) Bekker, H.; Berendsen, H.; Dijkstra, E.; Achterop, S.; Vondrumen, R.; VANDERSPOEL, D.; Sijbers, A.; Keegstra, H.; Renardus, M. Gromacs-a parallel computer for molecular-dynamics simulations. *4th International Conference on Computational Physics (PC 92)*; World Scientific Publishing, 1993; pp 252–256.
- (55) Babin, V.; Leforestier, C.; Paesani, F. Development of a “first principles” water potential with flexible monomers: Dimer potential energy surface, VRT spectrum, and second virial coefficient. *J. Chem. Theor. Comput.* **2013**, *9*, 5395–5403.
- (56) Bussi, G.; Donadio, D.; Parrinello, M. Canonical sampling through velocity rescaling. *J. Chem. Phys.* **2007**, *126*, 014101.
- (57) Parrinello, M.; Rahman, A. Crystal structure and pair potentials: A molecular-dynamics study. *Phys. Rev. Lett.* **1980**, *45*, 1196.



- (58) Hockney, R.; Eastwood, J. *Computer Simulations Using Particles*; McGraw-Hill: New York, 1981.
- (59) Abascal, J. L. F.; Sanz, E.; García Fernández, R.; Vega, C. A potential model for the study of ices and amorphous water: TIP4P/Ice. *J. Chem. Phys.* **2005**, *122*, 234511.
- (60) Russo, J.; Tanaka, H. Understanding water's anomalies with locally favoured structures. *Nat. Commun.* **2014**, *5*, 3556.
- (61) Ceriotti, M. Unsupervised machine learning in atomistic simulations, between predictions and understanding. *J. Chem. Phys.* **2019**, *150*, 150901.
- (62) Behler, J.; Parrinello, M. Generalized neural-network representation of high-dimensional potential-energy surfaces. *Phys. Rev. Lett.* **2007**, *98*, 146401.
- (63) Chau, P.-L.; Hardwick, A. J. A new order parameter for tetrahedral configurations. *Mol. Phys.* **1998**, *93*, 511–518.
- (64) Lynden-Bell, R. M.; Debenedetti, P. G. Computational investigation of order, structure, and dynamics in modified water models. *J. Phys. Chem. B* **2005**, *109*, 6527–6534.
- (65) Poli, E.; Jong, K. H.; Hassanali, A. Charge transfer as a ubiquitous mechanism in determining the negative charge at hydrophobic interfaces. *Nat. Commun.* **2020**, *11*, 901.
- (66) Maksimov, D.; Baldauf, C.; Rossi, M. The conformational space of a flexible amino acid at metallic surfaces. *Int. J. Quantum Chem.* **2021**, *121*, No. e26369.
- (67) Grant, W. Network Modularity and Local Environment Similarity as Descriptors of Protein Structure. Ph.D. Thesis, University of Cambridge, 2020.
- (68) De, S.; Bartók, A. P.; Csányi, G.; Ceriotti, M. Comparing molecules and solids across structural and alchemical space. *Phys. Chem. Chem. Phys.* **2016**, *18*, 13754–13769.
- (69) Bartók, A. P.; Kermode, J.; Bernstein, N.; Csányi, G. Machine learning a general-purpose interatomic potential for silicon. *Phys. Rev. X* **2018**, *8*, 041048.
- (70) Reinhardt, A.; Pickard, C. J.; Cheng, B. Predicting the phase diagram of titanium dioxide with random search and pattern recognition. *Phys. Chem. Chem. Phys.* **2020**, *22*, 12697–12705.
- (71) Himanen, L.; Jäger, M. O. J.; Morooka, E. V.; Federici Canova, F.; Ranawat, Y. S.; Gao, D. Z.; Rinke, P.; Foster, A. S. Dscribe: Library of descriptors for machine learning in materials science. *Comput. Phys. Commun.* **2020**, *247*, 106949.
- (72) Camisasca, G.; Schlesinger, D.; Zhovtobriukh, I.; Pitsevich, G.; Pettersson, L. G. M. A proposal for the structure of high- and low-density fluctuations in liquid water. *J. Chem. Phys.* **2019**, *151*, 034508.
- (73) Capelli, R.; Muniz-Miranda, F.; Pavan, G. M. Ephemeral ice-like local environments in classical models of liquid water. **2021**, arXiv preprint arXiv:2112.02022.
- (74) Mika, S.; Schölkopf, B.; Smola, A. J.; Müller, K.-R.; Scholz, M.; Rätsch, G. Kernel PCA and De-noising in feature spaces. *Advances in Neural Information Processing Systems*; MIT Press, 1998; pp 536–542.
- (75) Jolliffe, I. Principal component analysis. *Encyclopedia of Statistics in Behavioral Science*; Wiley, 2005.
- (76) Kruskal, J. B. *Multidimensional Scaling*; SAGE, 1978.
- (77) Carli, M.; Sormani, G.; Rodriguez, A.; Laio, A. Candidate binding sites for allosteric inhibition of the SARS-CoV-2 main protease from the analysis of large-scale molecular dynamics simulations. *J. Phys. Chem. Lett.* **2020**, *12*, 65–72.
- (78) Camastra, F.; Staiano, A. Intrinsic dimension estimation: Advances and open problems. *Inf. Sci.* **2016**, *328*, 26–41.
- (79) Tenenbaum, J. B.; Silva, V. d.; Langford, J. C. A global geometric framework for nonlinear dimensionality reduction. *science* **2000**, *290*, 2319–2323.
- (80) Roweis, S. T.; Saul, L. K. Nonlinear dimensionality reduction by locally linear embedding. *science* **2000**, *290*, 2323–2326.
- (81) Carreira-Perpinan, M. A. Mode-finding for mixtures of Gaussian distributions. *IEEE Trans. Pattern Anal. Mach. Intell.* **2000**, *22*, 1318–1323.
- (82) Gasparotto, P.; Ceriotti, M. Recognizing molecular patterns by machine learning: An agnostic structural definition of the hydrogen bond. *J. Chem. Phys.* **2014**, *141*, 174110.
- (83) Gasparotto, P.; Meißner, R. H.; Ceriotti, M. Recognizing local and global structural motifs at the atomic scale. *J. Chem. Theor. Comput.* **2018**, *14*, 486–498.
- (84) Geissler, P. L.; Dellago, C.; Chandler, D. Kinetic pathways of ion pair dissociation in water. *J. Phys. Chem. B* **1999**, *103*, 3706–3710.
- (85) Glielmo, A.; Husic, B. E.; Rodriguez, A.; Clementi, C.; Noé, F.; Laio, A. Unsupervised Learning Methods for Molecular Simulation Data. *Chem. Rev.* **2021**, *121*, 9722.
- (86) McInnes, L.; Healy, J.; Melville, J. Umap: Uniform manifold approximation and projection for dimension reduction. **2018**, arXiv preprint arXiv:1802.03426.
- (87) Becht, E.; McInnes, L.; Healy, J.; Dutertre, C.-A.; Kwok, I. W. H.; Ng, L. G.; Ginhoux, F.; Newell, E. W. Dimensionality reduction for visualizing single-cell data using UMAP. *Nat. Biotechnol.* **2019**, *37*, 38–44.
- (88) Zhang, C.; Galli, G. Dipolar correlations in liquid water. *J. Chem. Phys.* **2014**, *141*, 084504.
- (89) Diaz-Papkovich, A.; Anderson-Trocmé, L.; Ben-Eghan, C.; Gravel, S. UMAP reveals cryptic population structure and phenotype heterogeneity in large genomic cohorts. *PLoS Genet.* **2019**, *15*, No. e1008432.
- (90) Shiratani, E.; Sasai, M. Molecular scale precursor of the liquid-liquid phase transition of water. *J. Chem. Phys.* **1998**, *108*, 3264–3276.
- (91) Singh, R. S.; Biddle, J. W.; Debenedetti, P. G.; Anisimov, M. A. Two-state thermodynamics and the possibility of a liquid-liquid phase transition in supercooled TIP4P/2005 water. *J. Chem. Phys.* **2016**, *144*, 144504.
- (92) Adu-Offei Danso, A. H.; Rodriguez, A. Manuscript in preparation.